Published in final edited form as:

IEEE Trans Ultrason Ferroelectr Freq Control. 2015 December ; 62(12): 2068–2078.

Removal of Residual Cavitation Nuclei to Enhance Histotripsy Fractionation of Soft Tissue

Alexander P. Duryea[1], **Charles A. Cain**[1], **William W. Roberts**[1,2], and **Timothy L. Hall**[1]

[1]Department of Biomedical Engineering, University of Michigan, Ann Arbor, MI, USA

[2]Department of Urology, University of Michigan, Ann Arbor, MI, USA

Abstract

Remnant bubble nuclei generated by primary cavitation collapse can limit the efficiency of histotripsy soft tissue fractionation. When these residual bubbles persist from one histotripsy pulse to the next, they can seed the repetitive nucleation of cavitation bubbles at a discrete set of sites within the focal volume. This effect—referred to as cavitation memory—manifests in inefficient lesion formation, as certain sites within the focal volume are overtreated while others remain undertreated. While the cavitation memory effect can be passively mitigated by using a low pulse repetition frequency (PRF) that affords remnant nuclei sufficient time for dissolution between successive pulses, this low PRF also results in slow lesion production. As such, it would be highly desirable to maintain the high per-pulse efficiency associated with low pulse rates when much higher PRFs are utilized. In this vein we have developed a strategy for the active removal of the remnant bubble nuclei following primary cavitation collapse, using low amplitude ultrasound sequences (termed bubble removal sequences) to stimulate the aggregation and subsequent coalescence of these bubbles. In this study, bubble removal sequences were incorporated in high-PRF histotripsy treatment (100 Hz) of a red blood cell tissue-mimicking phantom that allows for the visualization of lesion development in real-time. A series of reference treatments were also conducted at the low PRF of 1 Hz in order to provide a point of comparison when cavitation memory effects are minimal. It was found that bubble removal sequences as short as 1 ms are capable of maintaining the efficacious lesion development characteristics associated with the low PRF of 1 Hz when the much higher pulse rate of 100 Hz is used. These results were then extended to the treatment of a large volume within the tissue phantom, and optimal bubble removal sequences identified for the single-focal-spot case were utilized to homogenize a 10 × 10 mm region at high rate.

INTRODUCTION

Primary cavitation generated by a high intensity acoustic pulse can produce an extensive set of residual bubble nuclei upon its collapse [1–9], with a single primary bubble fragmenting to yield dozens of microscopic (< 10 μm [10–12]) remnant daughters [1, 4, 7, 8]. These residual daughter bubbles can persist from tens of milliseconds [6, 13] up to full seconds [3,

DISCLOSURES

A.P. Duryea, W.W. Roberts, C.A. Cain, and T.L. Hall have financial interests and/or other relationships with HistoSonics, Inc., which has licensed intellectual property related to this manuscript.

7, 8, 14] and, if additional acoustic pulses are applied prior to their dissolution, can serve as nuclei to seed subsequent cavitation activity [1–3, 5, 6]. In this way remnant bubble nuclei impart a cavitation memory to their host medium. The threshold, extent, and distribution of ensuing cavitation events are all highly dependent on the bubble nuclei environment preceding an acoustic pulse [9, 15–19].

Previous work by Wang, *et al.* [9] has documented that this cavitation memory effect can limit the efficacy of histotripsy soft tissue fractionation when high pulse repetition frequencies (PRFs) are used. When applied at low PRF (< 10 Hz), the majority of remnant bubble nuclei generated by histotripsy bubble cloud collapse have sufficient time to dissolve between successive pulses. This permits each histotripsy pulse to nucleate cavitation at a randomized set of sites within the focal volume and produces highly efficient destruction of the targeted region. In contrast, when applied at high PRF (> 10 Hz) remnant bubble nuclei persist between successive histotripsy pulses and seed repetitive nucleation of cavitation at a discrete set of sites within the focus. This results in inefficient lesion formation, as sites with cavitation memory are over-treated while those without cavitation memory remain under-treated. Lesions generated in this fashion require an excess number of pulses to achieve complete destruction of the focal volume.

Our recent work has focused on developing a novel strategy for the active removal of the remnant bubble nuclei generated by primary cavitation collapse [12, 20]. It has been shown that when the population of residual bubbles is sonicated using a low amplitude (MI ≤ 1) ultrasound pulse, forces develop that promote their aggregation and subsequent coalescence. These pulses—which we term bubble removal sequences—are hypothesized to operate via an interplay of the primary and secondary Bjerknes forces, with the latter being the dominant facilitator of the process [12, 20]. Through the selection of appropriate bubble removal sequence parameters, a population of thousands of microscopic daughter bubbles generated by histotripsy bubble cloud collapse can be consolidated to a countably-small number of residuals. In this way we can actively clear the field of most remnant nuclei prior to delivery of subsequent histotripsy pulses, providing a ‘clean-slate’ for the nucleation of ensuing cavitation activity.

In the present study, we apply bubble removal sequences during histotripsy treatment of soft tissue-mimicking phantoms in an effort to alleviate the cavitation memory effect and improve the efficiency of lesion development at high pulse rates. Previous work has demonstrated that cavitation memory can be eliminated by waiting a sufficient duration between successive histotripsy pulses such that remnant nuclei can passively dissolve [9]. While this strategy produces a high per-pulse efficiency, the total time to produce a complete lesion is still long due to the low pulse rate. We therefore seek to maintain the high per-pulse efficiency associated with low pulse rates when much higher PRFs are utilized. Red blood cell tissue-mimicking phantoms were treated at the high PRF of 100 Hz with and without the incorporation of bubble removal sequences, and the resulting lesion development was optically monitored and quantified. A series of reference treatments was also conducted at the very low PRF of 1 Hz in order to establish a point of comparison when cavitation memory is minimal. Finally, the results obtained from single-focal-spot

treatments were extended to the treatment of a large volume, and optimal bubble removal parameters were utilized to homogenize a 10 × 10 mm region at high rate.

METHODS

A. Tissue Phantom Preparation

Experiments conducted in this study utilized a red blood cell (RBC) tissue-mimicking phantom designed for the visualization and quantification of cavitation-induced damage [21]. Fresh bovine blood was obtained from a local abattoir (Dunbar Meats, Milan, MI) and immediately mixed with a citrate-phosphate-dextrose (CPD) anticoagulant solution (C7165, Sigma-Aldrich, St. Louis, MO) in a blood-to-CPD ratio of 9:1 (v:v). Blood samples were subsequently stored in a refrigeration unit at 4 °C prior to use within 3 weeks of harvest. RBC tissue-mimicking phantoms were prepared following the procedures detailed by Maxwell, *et al*. [21]. Briefly, a three-layer agarose hydrogel was constructed using powdered agarose (AG-SP, LabScientific, Livingston, NJ) and 0.9% saline in a 1:100 ratio (w:v). The outer layers of the construct were composed solely of this transparent agarose hydrogel, while the very thin (< 0.5 mm) center layer contained agarose hydrogel with RBCs embedded in a concentration of 5%. In this study, the RBC tissue-mimicking phantoms were cast in the form of right cylinders with outer dimensions measuring 6 cm in diameter and 9 cm in height. The RBC-layer was located in the center of the cylinder oriented parallel to the cylinder axis. A mold constructed from ABS plastic on a fused deposition modeling (FDM) machine (Dimension Elite, Stratasys Ltd., Eden Prairie, MN) was used to create this geometry. The top portion of the mold was detachable such that, following gel solidification, it could be removed to allow for unimpeded acoustic access to the RBC-layer (see Fig. 1). Cavitation-induced damage to this RBC-layer manifests in an optical change from translucent red to transparent and colorless as a result of RBC lysis, providing real-time visual feedback for histotripsy lesion development [21].

B. Experimental Setup

The experimental setup used to study the impact of bubble removal sequences on histotripsy soft tissue fractionation is displayed in Fig. 1. All experiments were conducted in a water tank measuring 58 × 43 × 45 cm (L × W × H), which was filled with degased deionized water (dissolved oxygen content of 1.5 ± 0.2 mg/L at 23.0 ± 0.7 °C, corresponding to 16 ± 1% of saturation). Dissolved oxygen levels were measured at the beginning and end of each treatment day (n = 6) using a Traceable Digital Oxygen Meter (Control Co., Friendswood, TX).

A 500 kHz histotripsy transducer constructed in-house was used to deliver histotripsy therapy to the tissue phantoms treated in this study. It consisted of 112 individual watertight modules arranged in a spherical cap pattern with a 150 mm radius of curvature and 270 mm aperture. This geometry was maintained via a scaffold fabricated from Accura 60 plastic (3D Systems Inc., Rock Hill, SC) on a stereolithography machine. Individual module housings were also fabricated from Accura 60 using stereolithography. Within each, two 1-MHz Pz36 disc elements (Ferroperm Piezoceramics A/S, Kvistgaard, Denmark) measuring 20 mm in diameter and 1.6 mm in thickness were stacked and driven in unison to produce a

500-kHz equivalent source. Epoxy adhesive (Hysol E-120 HP, Loctite Corporation, Rocky Hill, CT) was used to bond the individual Pz36 elements together, as well as mate the front face of each stack to a flat Accura-60 disc. The latter served to provide both electrical insulation and acoustic matching between the elements and water. A marine grade epoxy (TAP Epoxy System 314 Resin/143 Hardener, TAP Plastics Inc., San Leandro, CA) was used to pot the back of each module, ensuring complete electrical insulation from the surrounding water. Overall, this arrangement of 112 modules produced a focal zone having -6-dB beamwidths measuring 2.0 mm in the lateral dimension and 6.3 mm in the axial. These measurements were conducted at a pressure amplitude of 8 MPa (linear regime) using a fiber optic hydrophone with a 100-μm-diameter sensing tip [22]. The histotripsy transducer was driven using a pulse amplifier developed in our lab, which was designed to produce very short, intense bursts. More details regarding the acoustic output generated by this setup are provided in the subsequent section.

A separate 1 MHz transducer—which we denote as the bubble removal module—was used to sonicate residual bubble nuclei produced by collapse of the histotripsy bubble cloud. It consisted of a single 1 MHz PZT-4 disc element (Steiner & Martins Inc., Miami, FL) measuring 50 mm in diameter and 2 mm in thickness. This frequency was selected based on our previous observation that bubble removal sequences of higher frequency (>500 kHz) produce more effective consolidation of residual nuclei following histotripsy bubble cloud collapse [12]. Similar to the histotripsy modules, the PZT-4 element was sealed within a stereolithography-fabricated Accura-60 housing. In this case the front face of the housing contained an acoustic lens having a focal length of 175 mm; this design was utilized to center the beam of the bubble removal module coincident with the histotripsy focus when the module was held within a central port in the histotripsy transducer scaffold (Fig. 1). The PZT-4 element was matched to the lens using an epoxy (1C-LV Hysol, Loctite Corporation, Rocky Hill, CT) filled 50 mesh copper screen (McMaster-Carr, Aurora, OH) to achieve the proper thickness and impedance. This arrangement produced an acoustic field with -6-dB beamwidths measuring 7.0 mm in the lateral dimension and exceeding 100 mm in the axial; as such, the bubble removal field fully encompassed the focal zone generated by the histotripsy transducer. These field scans were performed at a pressure amplitude of 300 kPa (linear regime) using an HNR-0500 needle hydrophone (Onda Corporation, Sunnyvale, CA). The bubble removal module was driven using a class-D amplifier developed in our lab; further details on the acoustic output are presented in the subsequent section.

As indicated in Fig. 1, the tissue-mimicking phantom was positioned below the histotripsy transducer such that the RBC layer was oriented vertically within the water tank (i.e. RBC layer parallel to the transducer axis). This allowed for visualization of the axial profile of histotripsy lesion development. Alignment of the histotripsy focus to the RBC layer was achieved via ultrasound imaging (not pictured in Fig. 1). An imaging probe (GE 11L with GE Logiq P6 system, GE Healthcare, Waukesha, WI) was oriented orthogonal to the RBC plane such that the layer showed as a thin hyperechoic strip on the ultrasound image. A test treatment was then performed in which a histotripsy bubble cloud was generated within the tissue phantom. This bubble cloud also showed as a hyperechoic zone in the image, and its location was marked with a cursor on the imager screen. In all subsequent treatments the RBC layer was aligned to this cursor location prior to sonication. For reference, the bubble

cloud generated by the histotripsy parameters utilized in this study measured approximately 1 mm in the lateral dimension such that it spanned the entirety of the thin (< 0.5 mm) RBC layer.

Histotripsy lesion development in the RBC tissue-mimicking phantom was monitored using a Photron Fastcam SA1.1 high speed camera (Photron USA Inc., San Diego, CA) equipped with a 200 mm macro lens (AF Micro-Nikkor 200mm f/4D IF-ED, Nikon Corporation, Tokyo, Japan). A large-area, high-power LED light source (Bridgelux 50C10K, Bridgelux Inc., Livermore, CA) was used to backlight the experiments such that bubbles generated in the phantom were visible as dark shadows on the optical images. Consistent with previous work [9, 21, 23], damage to the RBC layer showed as an optical change from translucent to transparent, allowing for real time monitoring of lesion development via this setup. Two images were acquired for each histotripsy pulse, each with an exposure time of 49 μs. The first image was taken 50 μs prior to histotripsy pulse firing to capture the RBC phantom without cavitation bubbles. For the very first pulse, this frame corresponded to the intact background that was used to normalize all frames in our image processing algorithm (*Section D*); for all subsequent pulses, this frame corresponded to the lesion resulting from the preceding pulse. The second image was acquired 120 μs following histotripsy pulse firing, which was empirically determined to capture the histotripsy bubble cloud near the point of maximum expansion. This time point corresponds to approximately 20 μs after the histotripsy pulse arrives at the focus.

C. Acoustic Pulse Sequence

Two general types of acoustic pulses were utilized in this study, as represented in Figs. 2(A) and 2(B): 1) Histotripsy pulses generated by the 500 kHz histotripsy transducer were used to initiate a cavitational bubble cloud to mechanically fractionate the tissue phantom; 2) Bubble removal sequences produced by the 1 MHz bubble removal module were used to sonicate residual nuclei following histotripsy bubble cloud collapse, stimulating their removal from the field. The overall timing of this pulse scheme is displayed in Fig. 2(C), with specifics provided henceforth.

Histotripsy pulses used in this study were very short (approximately 5 μs), had a center frequency of 500 kHz, and a peak-negative pressure (P−) of 33 MPa. The representative waveform displayed in Fig. 2(A), which was measured using the same fiber optic hydrophone used to perform histotripsy field scans, demonstrates the general shape of a histotripsy pulse. However, it was acquired at a lower P− of 12 MPa, as calibration at higher amplitudes can result in instantaneous cavitation on the fiber tip. The therapy P− of 33 MPa reported here was estimated via extrapolation based on the observation that P− increases extremely linearly with the transducer driving voltage. As previous work has established that histotripsy lesion development characteristics are highly dependent on pulse repetition frequency (PRF) [9], histotripsy PRFs of 1 and 100 Hz were tested. The low PRF of 1 Hz serves as a reference for lesion development when cavitation memory effects are minimal, while the high PRF of 100 Hz provides a scenario in which remnant bubble nuclei persist between successive pulses and cavitation memory is pronounced. 500 histotripsy pulses were applied to generate each lesion in this study.

A partial segment of a representative bubble removal sequence is displayed in Fig. 2(B), acquired using the same HNR-0500 needle hydrophone used to perform bubble removal module field scans. All bubble removal sequences had a center frequency of 1 MHz and amplitude of either 0 (i.e., no bubble removal) or 1 MPa. The latter setting was selected based on the results of a coarse amplitude investigation. To investigate the effect of pulse duration, bubble removal sequences of 10, 100, 1000, and 5000 cycles were tested. In all cases, a delay of 500 μs was imposed following histotripsy pulse firing to allow for unimpeded bubble cloud collapse prior to sonication with the bubble removal sequences (Fig. 2(C)). Eight histotripsy lesions were generated with each parameter combination tested in this study.

D. Histotripsy Lesion Development Quantification

Because the goal of this work is to recover the efficacious histotripsy lesion generation characteristics associated with low PRF (e.g. 1 Hz) when much higher PRFs are used (e.g. 100 Hz), the results of this study were analyzed in the context of a 1 Hz reference lesion. This reference lesion represents the average outcome of eight treatments conducted at the very low rate of 1 Hz, and was generated using the following algorithm: 1) The image frames containing the final lesions produced from the eight 1 Hz treatments were normalized, dividing by an image of the untreated field of view acquired prior to each respective treatment. 2) Each normalized image was converted to binary by setting pixels that resided above a threshold value to 1 and those below the threshold to 0; this threshold was selected as 1.5 for all cases (empirically determined based on image histograms). 3) The spatial location of binary lesions #2–8 were registered with that of binary lesion #1 by performing a two-dimensional cross correlation to determine the appropriate amount to shift each image. This accounted for any minor variations in alignment of the high speed camera to the histotripsy transducer focus. 4) All eight registered binary images were summed, and the 1 Hz reference lesion was defined as the collection of pixels with values >4 (i.e. the set of sites where damage was present in over half of the eight individual lesions). This reference lesion was also a binary image, with pixels exceeding the 4-count threshold set to 1 and all others set to 0. Fig. 3(A) shows the result.

As discussed with respect to the optical setup in Section B, a lesion image was acquired corresponding to each histotripsy pulse in a given treatment. These frames were normalized and thresholded using an algorithm analogous to that described above to create a set of binary images. Each resulting binary image was then registered to the 1 Hz reference lesion, again using a two-dimensional cross correlation between the reference lesion and the final lesion of interest to determine the appropriate translation. An example of the result of this processing for a lesion produced after 500 pulses at a PRF of 100 Hz without bubble removal is displayed in Fig. 3(B). As indicated in Fig 3(C), pixels that coincided with those of the 1 Hz reference lesion were defined as reference zone damage; those that were located outside the 1 Hz reference lesion were defined as peripheral zone damage. All 500 lesion images corresponding to a given treatment were analyzed in this way such that lesion development within the reference and peripheral zones could be quantified.

E. Volume Treatments

As an extension of this investigation, the bubble removal parameters identified to produce optimal histotripsy lesion development in the single-focus case were utilized to conduct histotripsy volume treatments within the RBC tissue-mimicking phantom. For these experiments the RBC-layer was constructed perpendicular to the axis of the cylindrical phantom, while the cylinder axis was maintained parallel to that of the transducer as shown in Fig. 1. This allowed for visualization of the lateral profile of the histotripsy lesion. A 10 × 10 mm region was treated within this lateral plane; in all cases, the transducer was maintained stationary while the tissue phantom was translated via a motorized positioning system (Anaheim Automation Inc., Anaheim, CA) through a series of 10 mm motion paths with 0.25 mm spacing. Histotripsy was applied continuously at a PRF of 100 Hz as the tissue phantom was mechanically scanned through this pattern. In order to vary the treatment dose, the speed of the positioning system was set to 1, 2, or 3 mm/s. For each dose four trials were conducted with and without the incorporation of optimal bubble removal sequences. Following treatment the tissue phantom was placed on a light box and photographed using a digital SLR camera (Rebel XT, Canon U.S.A. Inc., Melville, NY). Resulting images were processed in Matlab using the following algorithm: Each image was first converted to grayscale and then thresholded at six standard deviations above the background mean to create a binary image. Pixels residing below the threshold—which corresponded to unfractionated RBC phantom—were summed to quantify the area of intact structure remaining within the 10 × 10 mm target zone.

RESULTS

Representative lesions resulting from 500 pulse histotripsy treatments in the RBC tissue-mimicking phantom are displayed in Fig. 4, while lesion development within the reference and peripheral zones is quantified in Fig. 5 and Fig. 6, respectively. All treatments tested in this study produced lesions characterized by a completely fractionated central zone with varying degrees of damage in the periphery. The shape of the central lesion, extent of peripheral damage, and overall time-course of development were all highly dependent on the treatment parameters. As discussed in *Section D* of the Methods, because the goal of this work is to recover the efficacious histotripsy lesion generation characteristics associated with low PRF (1 Hz) when much higher PRF (100 Hz) is used, the lesions generated in this study were analyzed in the context of a 1 Hz reference lesion (Fig. 3). This paper has supplementary downloadable material available at http://ieeexplore.ieee.org, provided by the authors. This includes video sequences corresponding to histotripsy lesion development in the RBC tissue-mimicking phantom for the select cases of 1 Hz PRF, 100 Hz PRF, and 100 Hz PRF with 1000 cycle bubble removal. Each video displays two frames per histotripsy pulse (one capturing the bubble cloud and one capturing the lesion) as described in *Section B* of the Methods.

Without the incorporation of bubble removal sequences histotripsy lesion development showed a marked dependence on pulse rate. At the very low PRF of 1 Hz, histotripsy generated extremely homogeneous ellipsoidal-shaped lesions with smooth boundaries (Fig. 4(A)) and minimal damage in the peripheral zone (Fig. 6(A)). In contrast, treatment at the

high PRF of 100 Hz produced more heterogeneous lesions with jagged boundaries (Fig. 4(B)) and increased damage in the peripheral zone (Fig. 6(B)). The rate of lesion development within the reference zone—when evaluated as a function of pulse number—was significantly greater at the low PRF of 1 Hz (Fig. 5(A)) compared to the high PRF 100 Hz (Fig. 5(B)). Indeed, the number of histotripsy pulses required to achieve 50% damage within the reference zone was significantly lower at 1 Hz in comparison to 100 Hz (*t-test*, $P < 0.001$), with respective values of 65 ± 27 (mean ± SD) and 164 ± 57. This metric of per-pulse efficiency is displayed in Fig. 7.

The incorporation of bubble removal sequences in 100 Hz histotripsy treatments resulted in lesion generation characteristics that more closely approximated those achieved at the low PRF of 1 Hz, with the significance of the impact dependent on the bubble removal sequence duration. Relatively short bubble removal sequences of 10 and 100 cycles had moderate impact on lesion development characteristics, producing final lesions with appearance intermediate to that observed at 1 Hz and 100 Hz without bubble removal (Fig. 4(C) and Fig. 4(D)). In each case, the extent of damage within the peripheral zone was reduced relative to that observed at 100 Hz without bubble removal (Fig. 6(C) and Fig. 6(D)), while lesion development within the reference zone showed an increase in per-pulse efficiency (Fig. 5(C) and Fig. 5(D)). Treatments performed with 10 cycle bubble removal sequences required 104 ± 50 pulses to achieve 50% damage within the reference zone, while those with 100 cycle bubble removal sequences required 87 ± 31 pulses (Fig. 7). Both of these values represent a statistically significant reduction relative to the case of 100 Hz without bubble removal (*t-test*, $P < 0.04$).

Bubble removal sequences of 1000 and 5000 cycles had a drastic impact on lesion development at 100 Hz PRF, producing characteristics markedly similar to those observed at the much lower pulse rate of 1 Hz. Final lesions produced following these respective treatment schemes were ellipsoidal-shaped with smooth boundaries (Fig. 4(E) and Fig. 4(F)), closely approximating that produced following treatment at the low PRF of 1 Hz (Fig. 4(A)). In each case, damage in the peripheral zone was drastically reduced relative to 100 Hz without the incorporation of bubble removal sequences (Fig. 6(E) and Fig. 6(F)), again commensurate with that produced at the low PRF of 1 Hz. Lesion development within the reference zone was also augmented for each case (Fig. 5(E) and Fig. 5(F)), with per-pulse efficiencies that matched (5000 cycle bubble removal) or even exceeded (1000 cycle bubble removal) that produced at the low PRF of 1 Hz. Specifically, with the incorporation of 1000 cycle bubble removal sequences 46 ± 16 pulses were required to achieve 50% damage within the reference zone; using 5000 cycle bubble removal sequences 69 ± 32 pulses were necessary to reach this same level. Both of these values again represent statistically significant reductions relative to the case of 100 Hz without bubble removal (*t-test*, $P < 0.001$).

As an extension of this investigation, the 1000 cycle bubble removal sequence identified to produce optimal histotripsy lesion development for the single-focal-location case was utilized to conduct volume treatments within the RBC tissue-mimicking phantom (described in *Section E* of the Methods). Representative images showing the 10 × 10 mm target zone following treatment are displayed in Fig. 8. Without the incorporation of bubble removal

(Fig. 8, top row), as the histotripsy dose was reduced the area of intact phantom structure within the target zone was observed to increase (*t-test*, $P < 0.02$). Specifically, at linear scan speeds of 1, 2, and 3 mm/s, histotripsy treatment at 100 Hz PRF left behind 5.2 ± 2.8, 24.1 ± 7.9, and 40.5 ± 4.6 mm^2 of intact structure within the 10 × 10 mm target zone. With the incorporation of bubble removal (Fig. 8, bottom row), all histotripsy doses investigated resulted in near-complete homogenization of the target zone. The majority of remaining intact structure in these cases resided on the perimeter of the targeted volume, with scan speeds of 1, 2, and 3 mm/s producing residual structure areas of 0.9 ± 1.0, 4.0 ± 1.1, and 3.8 ± 1.6 mm^2, respectively. Each of these values represents a statistically significant reduction in comparison to its histotripsy-only counterpart (*t-test*, $P < 0.03$).

DISCUSSION

This study demonstrates a unique strategy for mitigating the efficiency-limiting effects of residual bubble nuclei in histotripsy soft tissue fractionation, using low-amplitude ultrasound pulses to stimulate their removal from the target medium. When histotripsy is applied in isolation, lesion generation characteristics in the tissue-mimicking RBC phantom are highly dependent on PRF. At the low PRF of 1 Hz, histotripsy lesion development displays a high per-pulse efficiency and the general appearance of final lesions is highly reproducible, having an ellipsoidal shape with smooth boundaries and minimal peripheral damage. In contrast, treatment at the high PRF of 100 Hz results in a pronounced reduction in the per-pulse efficiency of lesion development, and final lesions have a more heterogeneous structure with jagged boundaries and substantial damage in the periphery. With the introduction of bubble removal sequences, the efficacious lesion development characteristics associated with the low pulse rate of 1 Hz can be maintained when the much higher PRF of 100 Hz is used. The impact of this bubble removal strategy is dependent on the sequence duration, with the longer bubble removal sequences of 1000 and 5000 cycles achieving efficiencies and final lesion structures comparable to those observed at 1 Hz.

The bubble removal strategy utilized in this study has been the subject of our recent work [12, 20]. Through the application of low-amplitude (MI ≤ 1) ultrasound pulse sequences on the order of 1 ms in duration, the aggregation and subsequent coalescence of remnant bubble nuclei can be stimulated. This effect is attributed to a combination of the forces exerted by the acoustic field on individual bubbles (primary Bjerknes force) [24–29] and the forces exerted by bubbles on one another (secondary Bjerknes force) [24, 25, 28, 30]; the latter is hypothesized to be the dominant facilitator of the process [12, 20]. Sonication of the remnant nuclei generated by histotripsy bubble cloud collapse with a bubble removal sequence can consolidate the population from thousands of microscopic daughter bubbles to a countably small number of residuals. This has been shown to significantly reduce the area of remnant bubbles expanded by a secondary ‘interrogation’ ultrasound pulse [12, 20], as well as alleviate the attenuation of an acoustic pulse propagating through the medium [12]. It is important to note that these effects have been previously studied in water, where remnant bubble nuclei are free to translate and the bubble consolidation process experiences minimal impedance. The present study offers an interesting extension of this work, as the medium of interest is a tissue-mimicking phantom composed of agarose hydrogel. In a separate set of fast-frame high speed imaging experiments not included in this manuscript, we monitored

the bubble consolidation process within the agarose construct to evaluate the feasibility of bubble removal in this setting. It was observed that, after a minimal number of histotripsy pulses (< 10), the medium had undergone a sufficient degree of fractionation such that bubble nuclei could be driven through the agarose matrix and consolidation achieved. Interestingly, following only 10 histotripsy pulses the target volume is far from fully fractionated, suggesting that only a minimal degree of porosity is required to achieve the translation of these microscopic bubbles.

The results of this study corroborate previous work by Wang, *et al.* [9], in which the implications of remnant bubble nuclei in histotripsy soft tissue fractionation were explored. In their study, it was shown that the persistence of residual bubbles between successive histotripsy pulses results in the repetitive nucleation of cavitation at a discrete set of sites within the focal volume. This effect—referred to as cavitation memory—limits the efficiency of histotripsy soft tissue fractionation, resulting in the overtreatment of sites with cavitation memory while those without remain undertreated. Development of a histotripsy lesion in this manner requires an excess number of pulses to achieve complete homogenization of the focal volume. One straightforward strategy for mitigating the memory effect is to simply wait a sufficient time between successive histotripsy pulses such that remnant bubble nuclei can passively dissolve. Indeed, Wang, *et al*. demonstrated that the correlation coefficient between histotripsy cavitation patterns in successive pulses decreases exponentially as the time between pulses increases from 2–200 ms; correspondingly, the lesion development efficiency improves [9]. While this passive approach offers a means of augmenting per-pulse efficiency, the time-rate of treatment suffers when low PRFs are used. For this reason it is desirable to maintain the high efficiency associated with low pulse rates when much higher PRFs are utilized. The active approach provided by bubble removal sequences affords us with this capability, enabling high per-pulse efficiency to be maintained at high pulse rate.

While the cavitation memory effect limits the efficacy of histotripsy lesion development, it is possible that the persistence of a minimal subset of remnant bubble nuclei may augment the therapy. An interesting outcome of this study is the observation that histotripsy delivered at 100 Hz PRF with 5000 cycle bubble removal sequences closely matched the per-pulse efficiency achieved at the low PRF of 1 Hz, while histotripsy delivered at 100 Hz PRF with 1000 cycle bubble removal sequences exceeded it. One possible explanation for this observation is that the longer-duration 5000 cycle bubble removal sequence results in near-complete elimination of residual bubble nuclei, allowing lesion development to behave markedly similar to the 1 Hz case in which memory effects are expected to be negligible [6, 9]. In contrast, the shorter-duration 1000 cycle bubble removal sequence may not achieve complete consolidation of remnant bubbles, leaving behind a minimal number of coalesced seeding nuclei. These nuclei—which are likely to have been significantly redistributed following each bubble removal sequence—may then augment the subsequent histotripsy pulse. It is likely that the benefit gleaned from these residual bubbles is dependent on the histotripsy pulse amplitude, with pulses at or just below the cavitation threshold experiencing maximal benefit. Previous work has indicated that cavitation memory may indeed be beneficial in cavitation-based therapies that lack sufficient headroom to

consistently generate primary cavitation with each pulse, and the persistence of bubble nuclei may enhance the cavitation process in such cases [5, 31–33]. This idea has also been utilized in previous histotripsy studies to enhance tissue fractionation [34–36]. In the present work, our estimated P− of 33 MPa only marginally exceeds the previously measured inertial cavitation threshold in water [37], suggesting that the histotripsy pulses employed here may indeed benefit from a strategic seeding of the target medium. This concept may provide a useful tool in cases in which pulse headroom is limited, and as such warrants further study.

A natural extension of the single-focal-spot lesion development characterized in this study is the treatment of a large volume, as many applications of histotripsy soft tissue fractionation require the homogenization of a target zone much larger than a single histotripsy focus. In such cases the implications of cavitation memory remain pronounced, and the inhomogeneous tissue disruption that results from the persistence of remnant bubble nuclei can manifest in islands of structurally intact tissue persisting within the treatment volume [38, 39]. This phenomenon was observed in the volume treatments conducted in the RBC tissue-mimicking phantom in the present study (Fig. 8), with the extent of intact structure observed to increase with increasing scan rate (i.e. with decreasing histotripsy dose). If such volume treatments are being conducted with an electronically phasable array, the memory effect can be mitigated via strategic steering of the histotripsy focus [40]. Rather than treating adjacent points sequentially, it would be beneficial for successive treatment points to reside sufficiently far away from one another such that remnant nuclei do not influence the distribution of cavitation activity. However, in cases in which a steerable array is either not available or not feasible, the bubble removal strategy explored in this paper can provide a means of enhancing the efficacy of large volume treatments (Fig. 8). The enhanced lesion development efficiency afforded by bubble removal sequences (Fig. 5) permits the complete homogenization of a point within the target volume with a reduced histotripsy dose. Furthermore, the highly-reproducible lesion shape generated with bubble removal sequences (Fig. 4(E) and Fig. 4(F)) allows for improved treatment planning with respect to the scan path of the histotripsy transducer. The combination of these characteristics manifests in the capability of faster histotripsy treatment of large target volumes with a reduced probability of residual intact structure.

While this study presents an exciting strategy for mitigating the effects of residual bubble nuclei to enhance histotripsy soft tissue fractionation, several limitations do exist. This preliminary work utilized the RBC tissue-mimicking phantom due to its ability to provide real-time feedback of the histotripsy lesion development process. However, the results obtained in this phantom must be validated in biological tissues. Our future work will focus on this effort, evaluating the bubble removal process in *ex-vivo* tissue followed by eventual *in-vivo* application. As previous studies have demonstrated that the RBC phantom is an excellent predictor of the outcomes observed in soft tissue [9, 21, 23], we fully expect this process to translate to biological settings to enhance the efficacy of histotripsy when high pulse rates are used.

CONCLUSION

Microscopic residual bubble nuclei produced by primary cavitation collapse can limit the efficacy of histotripsy soft tissue fractionation by imposing cavitation memory to the target medium. Sites within the focal volume at which remnant nuclei persist between pulses will experience the repetitive nucleation of cavitation activity and become overtreated, while those without remnant nuclei remain undertreated and require an excess number of pulses for complete homogenization. This effect manifests in histotripsy treatment at low PRF achieving significantly greater per-pulse efficiency in comparison to high PRF, as low pulse rates afford remnant bubbles with sufficient time to dissolve. The bubble removal sequences explored in this study provide a means of actively mitigating the ill-effects of bubble nuclei and allow the histotripsy lesion development characteristics observed at the high PRF of 100 Hz to closely match those achieved at the very low PRF of 1 Hz. This includes not only the high per-pulse efficiency of lesion development, but also the homogeneous, reproducible shape of final lesions. Both of these characteristics are highly desirable when planning and conducting histotripsy treatment of a large target volume, and a major potential application of this strategy is enhancing the speed and completeness of volume ablation. Our future work will extend the results of this phantom study to the treatment of biological tissues, with the eventual goal of bubble removal sequences providing an adjunct to histotripsy treatment *in-vivo*.

ACKNOWLEDGMENTS

Research reported in this publication was supported by The National Institute of Diabetes and Digestive and Kidney Diseases of the National Institutes of Health under award number R01DK091267. The content is solely the responsibility of the authors and does not necessarily represent the official views of the National Institutes of Health.

REFERENCES

1. Flynn HG, Church CC. A mechanism for the generation of cavitation maxima by pulsed ultrasound. J Acoust Soc Am. 1984 Aug.76:505–512. [PubMed: 6481000]
2. Fowlkes JB, Crum LA. Cavitation threshold measurements for microsecond length pulses of ultrasound. The Journal of the Acoustical Society of America. 1988; 83:2190–2201. [PubMed: 3411016]
3. Huber P, Jochle K, Debus J. Influence of shock wave pressure amplitude and pulse repetition frequency on the lifespan, size and number of transient cavities in the field of an electromagnetic lithotripter. Phys Med Biol. 1998 Oct.43:3113–3128. [PubMed: 9814538]
4. Brennen CE. Fission of collapsing cavitation bubbles. Journal of Fluid Mechanics. 2002; 472:153–166.
5. Arora M, Junge L, Ohl CD. Cavitation cluster dynamics in shock-wave lithotripsy: part 1. Free field. Ultrasound Med Biol. 2005 Jun.31:827–839. [PubMed: 15936498]
6. Xu Z, Hall TL, Fowlkes JB, Cain CA. Optical and acoustic monitoring of bubble cloud dynamics at a tissue-fluid interface in ultrasound tissue erosion. The Journal of the Acoustical Society of America. 2007; 121:2421–2430. [PubMed: 17471753]
7. Pishchalnikov, YA.; McAteer, JA.; Pishchalnikova, IV.; Williams, JC.; Bailey, MR.; Sapozhnikov, OA. Bubble proliferation in shock wave lithotripsy occurs during inertial collapse; 18th International Symposium on Nonlinear Acoustics; 2008. p. 460-463.
8. Pishchalnikov YA, Williams JC, McAteer JA. Bubble proliferation in the cavitation field of a shock wave lithotripter. J Acoust Soc Am. 2011 Aug.130:EL87–EL93. [PubMed: 21877776]

9. Wang TY, Xu Z, Hall TL, Fowlkes JB, Cain CA. An efficient treatment strategy for histotripsy by removing cavitation memory. Ultrasound Med Biol. 2012 May.38:753–766. [PubMed: 22402025]
10. Pishchalnikov YA, McAteer JA, Williams JC Jr. Effect of firing rate on the performance of shock wave lithotriptors. BJU Int. 2008 Dec.102:1681–1686. [PubMed: 18710450]
11. Mettin R, Akhatov I, Parlitz U, Ohl CD, Lauterborn W. Bjerknes forces between small cavitation bubbles in a strong acoustic field. Physical Review E. 1997 Sep 01.56:2924–2931.
12. Duryea AP, Tamaddoni HA, Cain CA, Roberts WW, Hall TL. Removal of residual nuclei following a cavitation event: a parametric study. IEEE Trans Ultrason Ferroelectr Freq Control. 2015; 62:1605–1614.
13. Chen WS, Matula TJ, Crum LA. The disappearance of ultrasound contrast bubbles: observations of bubble dissolution and cavitation nucleation. Ultrasound Med Biol. 2002 Jun.28:793–803. [PubMed: 12113792]
14. Epstein PS, Plesset MS. On the stability of gas bubbles in liquid-gas solutions. The Journal of Chemical Physics. 1950; 18:1505–1509.
15. Arora M, Ohl CD, Lohse D. Effect of nuclei concentration on cavitation cluster dynamics. J Acoust Soc Am. 2007 Jun.121:3432–3436. [PubMed: 17552694]
16. Yavas O, Leiderer P, Park HK, Grigoropoulos CP, Poon CC, Tam AC. Enhanced acoustic cavitation following laser-induced bubble formation: Long-term memory effect. Physical Review Letters. 1994 Mar 28.72:2021–2024. [PubMed: 10055768]
17. Pishchalnikov YA, McAteer JA, Williams JC Jr, Pishchalnikova IV, Vonderhaar RJ. Why stones break better at slow shockwave rates than at fast rates: in vitro study with a research electrohydraulic lithotripter. J Endourol. 2006 Aug.20:537–541. [PubMed: 16903810]
18. Sapozhnikov OA, Khokhlova VA, Bailey MR, Williams JC Jr, McAteer JA, Cleveland RO, et al. Effect of overpressure and pulse repetition frequency on cavitation in shock wave lithotripsy. J Acoust Soc Am. 2002 Sep.112:1183–1195. [PubMed: 12243163]
19. Pishchalnikov YA, Sapozhnikov OA, Bailey MR, Pishchalnikova IV, Williams JC, McAteer JA. Cavitation selectively reduces the negative-pressure phase of lithotripter shock pulses. Acoust Res Lett Online. 2005 Nov 3.6:280–286. [PubMed: 19756170]
20. Duryea AP, Cain CA, Tamaddoni HA, Roberts WW, Hall TL. Removal of Residual Nuclei Following a Cavitation Event using Low-Amplitude Ultrasound. IEEE Trans Ultrason Ferroelectr Freq Control. 2014 Oct.61:1619–1626. [PubMed: 25265172]
21. Maxwell AD, Wang T-Y, Yuan L, Duryea AP, Xu Z, Cain CA. A tissue phantom for visualization and measurement of ultrasound-induced cavitation damage. Ultrasound in medicine & biology. 2010 Oct 28.36:2132–2143. [PubMed: 21030142]
22. Parsons JE, Cain CA, Fowlkes JB. Cost-effective assembly of a basic fiber-optic hydrophone for measurement of high-amplitude therapeutic ultrasound fields. J Acoust Soc Am. 2006 Mar. 119:1432–1440. [PubMed: 16583887]
23. Kuang-Wei L, Yohan K, Maxwell AD, Tzu-Yin W, Hall TL, Zhen X, et al. Histotripsy beyond the intrinsic cavitation threshold using very short ultrasound pulses: microtripsy. Ultrasonics, Ferroelectrics, and Frequency Control, IEEE Transactions on. 2014; 61:251–265.
24. Blake FG. Bjerknes Forces in Stationary Sound Fields. The Journal of the Acoustical Society of America. 1949; 21:551–551.
25. Neppiras EA. Subharmonic and Other Low-Frequency Emission from Bubbles in Sound-Irradiated Liquids. The Journal of the Acoustical Society of America. 1969; 46:587–601.
26. Crum LA, Eller AI. Motion of Bubbles in a Stationary Sound Field. The Journal of the Acoustical Society of America. 1970; 48:181–189.
27. Crum LA. The motion of bubbles in a stationary sound field. The Journal of the Acoustical Society of America. 1969; 46:1411.
28. Leighton, TG. The Acoustic Bubble. San Diego, CA: Academic Press Inc; 1997.
29. Leighton TG, Walton AJ, Pickworth MJW. Primary Bjerknes forces. European Journal of Physics. 1990; 11:47.
30. Crum LA. Bjerknes forces on bubbles in a stationary sound field. The Journal of the Acoustical Society of America. 1975; 57:1363–1370.

31. Delius M, Brendel W. A model of extracorporeal shock wave action: tandem action of shock waves. Ultrasound Med Biol. 1988; 14:515–518. [PubMed: 3227574]
32. Huber P, Debus J, Jochle K, Simiantonakis I, Jenne J, Rastert R, et al. Control of cavitation activity by different shockwave pulsing regimes. Phys Med Biol. 1999 Jun.44:1427–1437. [PubMed: 10498515]
33. Loske AM, Prieto FE, Fernandez F, van Cauwelaert J. Tandem shock wave cavitation enhancement for extracorporeal lithotripsy. Phys Med Biol. 2002 Nov 21.47:3945–3957. [PubMed: 12476975]
34. Xu Z, Fowlkes JB, Rothman ED, Levin AM, Cain CA. Controlled ultrasound tissue erosion: the role of dynamic interaction between insonation and microbubble activity. J Acoust Soc Am. 2005 Jan.117:424–435. [PubMed: 15704435]
35. Xu Z, Fowlkes JB, Cain CA. A new strategy to enhance cavitational tissue erosion using a high-intensity, Initiating sequence. IEEE Trans Ultrason Ferroelectr Freq Control. 2006 Aug.53:1412–1424. [PubMed: 16921893]
36. Parsons JE, Cain CA, Abrams GD, Fowlkes JB. Pulsed cavitational ultrasound therapy for controlled tissue homogenization. Ultrasound Med Biol. 2006 Jan.32:115–129. [PubMed: 16364803]
37. Maxwell AD, Cain CA, Hall TL, Fowlkes JB, Xu Z. Probability of Cavitation for Single Ultrasound Pulses Applied to Tissues and Tissue-Mimicking Materials. Ultrasound in Medicine & Biology. 2013 Mar.39:449–465. [PubMed: 23380152]
38. Roberts WW, Hall TL, Ives K, Wolf JS Jr, Fowlkes JB, Cain CA. Pulsed cavitational ultrasound: a noninvasive technology for controlled tissue ablation (histotripsy) in the rabbit kidney. J Urol. 2006 Feb.175:734–738. [PubMed: 16407041]
39. Wang TY, Xu Z, Winterroth F, Hall TL, Fowlkes JB, Rothman ED, et al. Quantitative ultrasound backscatter for pulsed cavitational ultrasound therapy- histotripsy. IEEE Trans Ultrason Ferroelectr Freq Control. 2009 May.56:995–1005. [PubMed: 19750596]
40. Hall, TL.; Michigan, Uo. Histotripsy: Non-Invasive Ultrasound Surgery. University of Michigan; 2007.

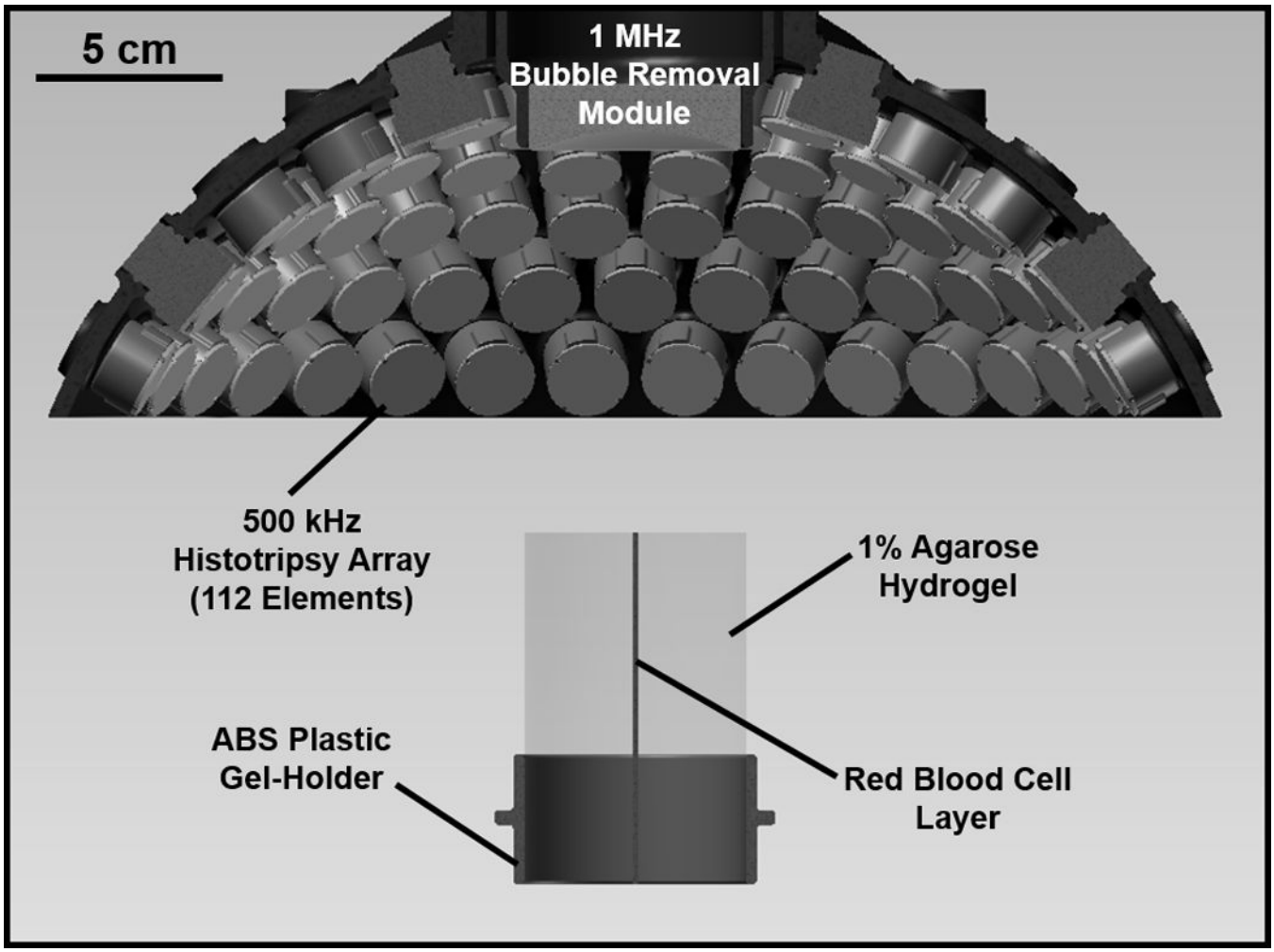

Fig. 1.

Experimental setup used to study the effect of bubble removal pulses on histotripsy fractionation of soft tissue. Histotripsy treatment was delivered from a transducer composed of 112 individual 500 kHz modules arranged in a spherical cap pattern, while a separate 1 MHz transducer aligned confocally with the histotripsy array was used to generate bubble removal pulses. Treatments were performed on a tissue phantom constructed from 1% agarose hydrogel with a thin layer of red blood cells (RBCs) embedded within. This RBC layer was oriented parallel to the transducer axis such that the axial profile of histotripsy lesion development could be visualized.

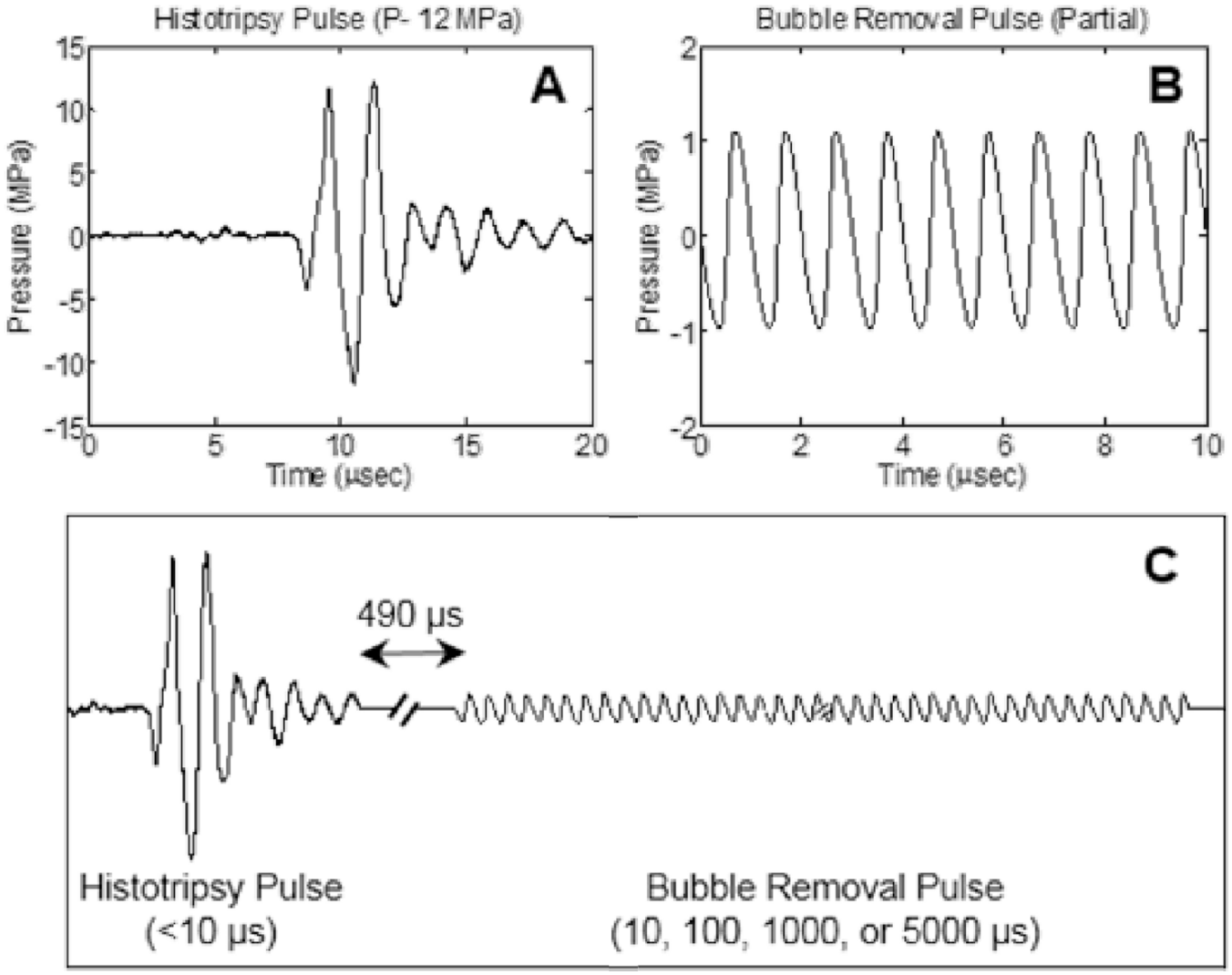

Fig. 2.

General pulse scheme used to study the effect of bubble removal pulses on histotripsy soft tissue fractionation. (A) Representative waveform acquired from the 500 kHz histotripsy transducer at low power (below the cavitation threshold). The histotripsy pulse P− used for tissue phantom treatments is estimated to be 33 MPa. (B) Partial segment of the bubble removal pulse; all bubble removal pulses had a center frequency of 1 MHz, and amplitude set to either 0 or 1 MPa. (C) Overall timing of the experimental pulse scheme. A 500 µs delay was imposed following histotripsy pulse firing to allow the bubble cloud to collapse in an unimpeded manner. Bubble removal pulse durations of 10, 100, 1000, and 5000 µs were investigated.

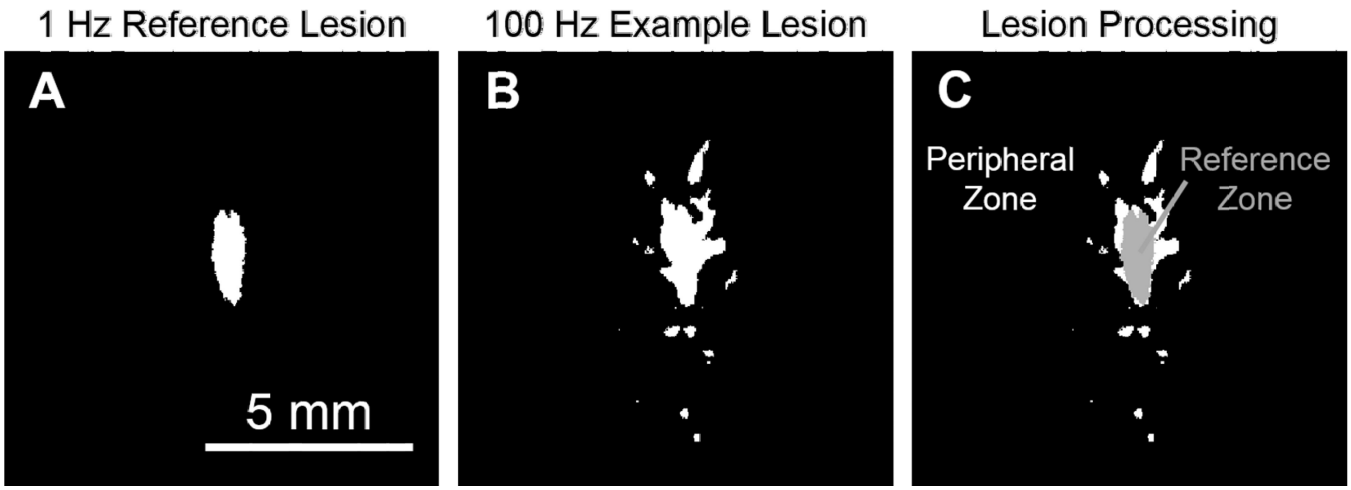

Fig. 3.

Image processing to quantify the course of lesion development. (A) Because the goal of this work is to recover the efficacious lesion development characteristics associated with low PRF when much higher PRFs are used, the results of this study were analyzed in the context of a 1 Hz reference lesion. This reference lesion represents an average lesion generated at the very low rate of 1 Hz (see text for details). (B) For a given lesion of interest, the corresponding image frame was normalized and thresholded to produce a binary image. A two-dimensional cross correlation was then performed to register the lesion with the 1 Hz reference for damage quantification. (C) Damage occurring within the area encompassed by the 1 Hz reference was defined as reference zone damage, while that falling outside of the 1 Hz reference was defined as peripheral zone damage. The lesion images corresponding to each of the 500 pulses in a given treatment were analyzed in this fashion such that the course of lesion development could be quantified.

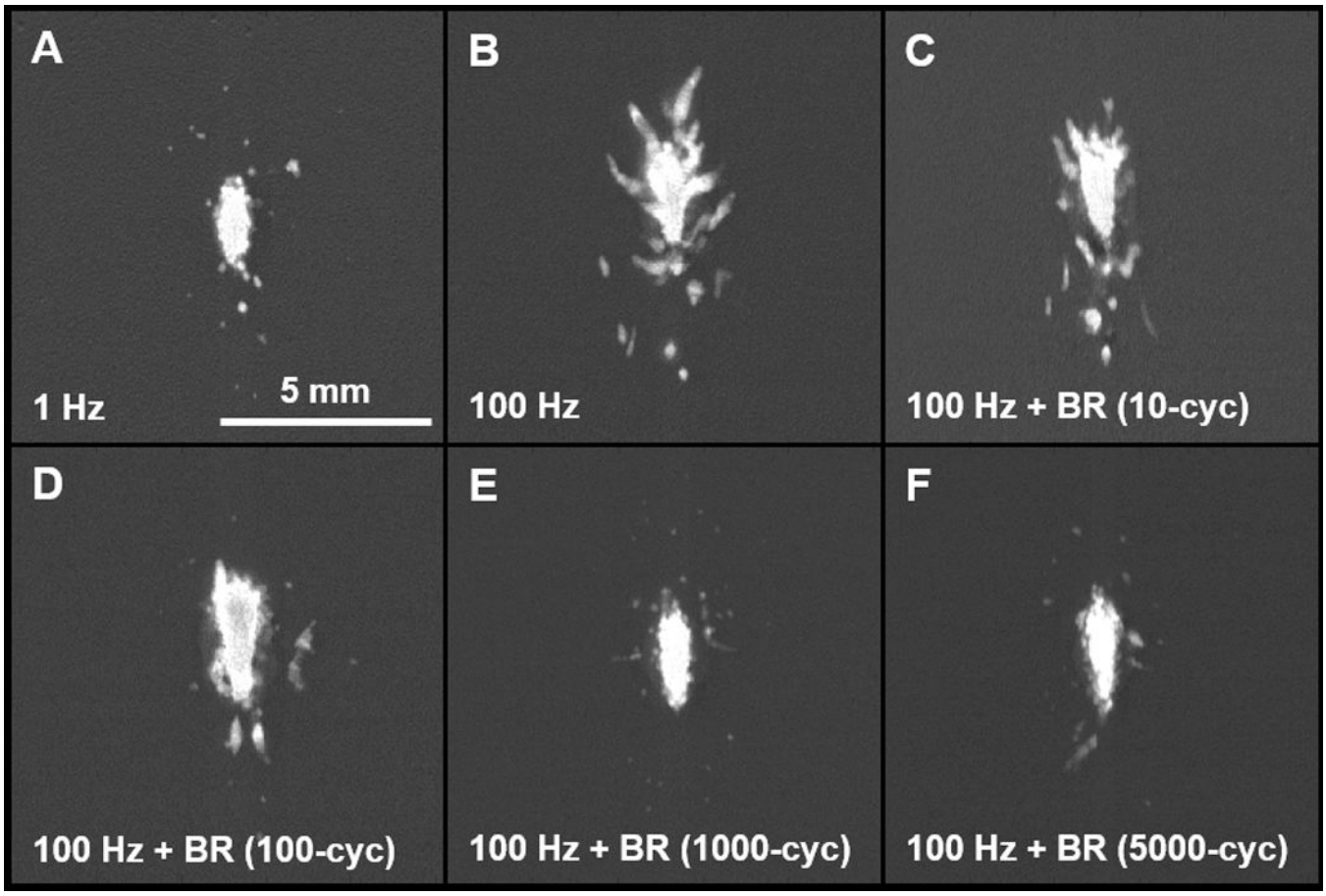

Fig. 4.

Representative lesions in the RBC tissue-mimicking phantom following 500 histotripsy pulses. All treatments tested in this study produced lesions characterized by a completely fractionated central zone with varying degrees of damage in the periphery. (A) The very low PRF of 1 Hz generated ellipsoidal-shaped lesions with smooth boundaries and minimal peripheral damage. (B) Treatment at the high PRF of 100 Hz produced heterogeneously-shaped lesions with jagged boundaries and increased peripheral damage. (C/D) At 100 Hz PRF, the incorporation of relatively short duration bubble removal sequences of 10 and 100 cycles resulted in final lesions with appearance intermediate to that observed at 1 Hz and 100 Hz without bubble removal. (E/F) Longer bubble removal sequences of 1000 and 5000 cycles allowed final lesions generated at 100 Hz to closely approximate those produced at the low rate of 1 Hz.

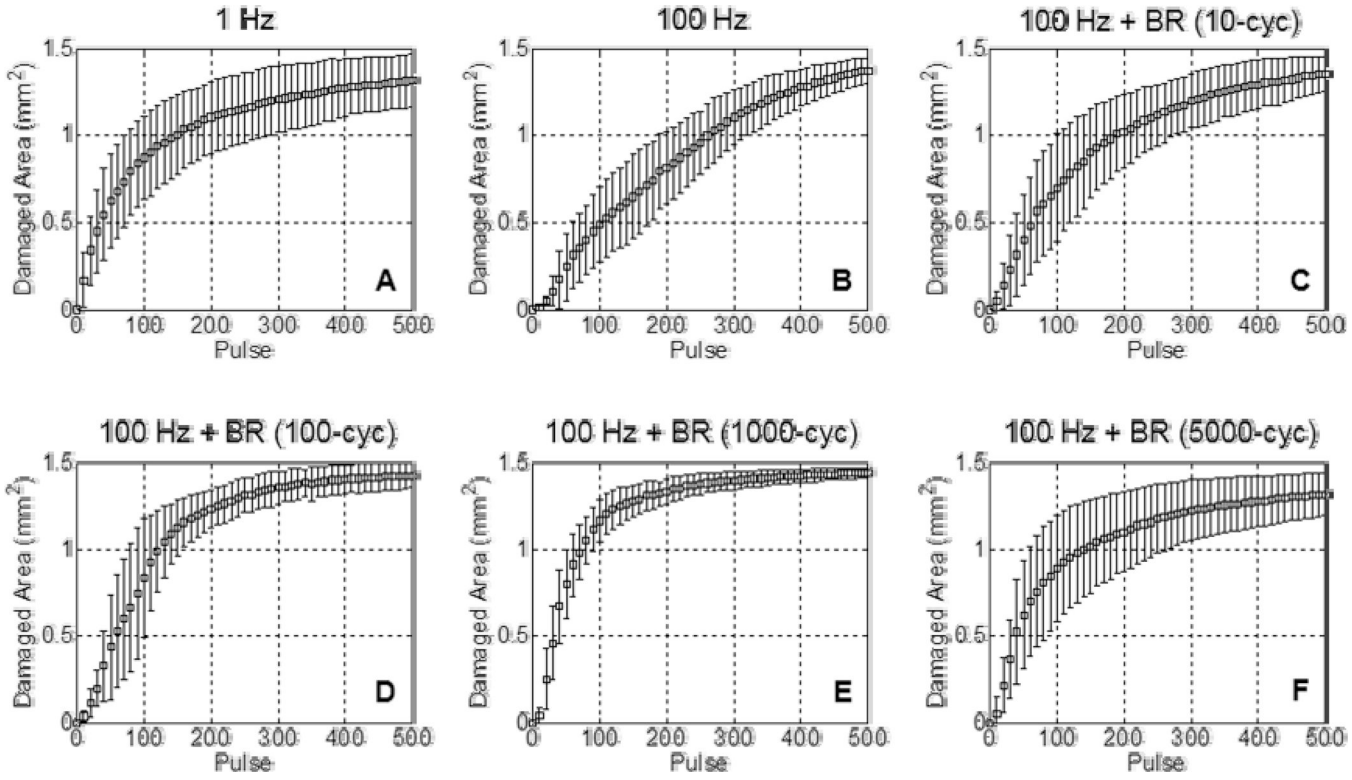

Fig. 5.

Lesion development within the reference zone over 500 histotripsy pulses. Each curve shows the mean ± SD over eight treatments. (A) The low PRF of 1 Hz produced lesions with a relatively high per-pulse efficiency. (B) At the much higher PRF of 100 Hz, lesion generation showed a reduction in per-pulse efficiency. (C–F) With the incorporation of bubble removal sequences, the efficiency of lesion development at the high PRF of 100 Hz was improved, more closely approximating that observed at the low pulse rate of 1 Hz. Optimal lesion development was observed with the incorporation of a 1000 cycle bubble removal sequence, which produced a per-pulse efficiency exceeding that observed at 1 Hz.

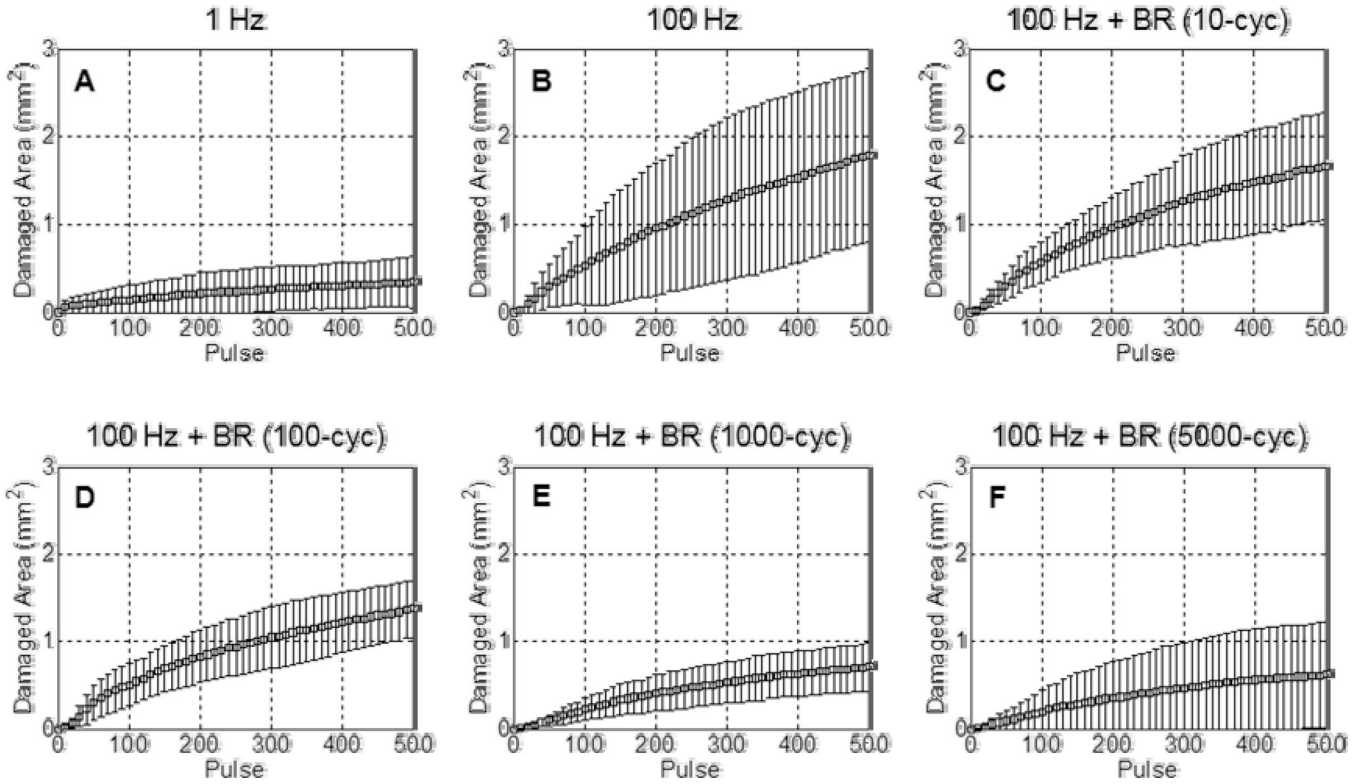

Fig. 6.

Lesion development within the peripheral zone over 500 histotripsy pulses. Each curve shows the mean ± SD over eight treatments. (A) The low PRF of 1 Hz produced lesions with minimal peripheral zone damage. (B) At the much higher PRF of 100 Hz, the extent of damage observed in the peripheral zone increased substantially. (C–F) With the incorporation of bubble removal sequences, the degree of damage in the peripheral zone produced at 100 Hz PRF was reduced. Bubble removal sequences of 1000 and 5000 cycles mitigated peripheral zone damage to levels commensurate with that observed at 1 Hz.

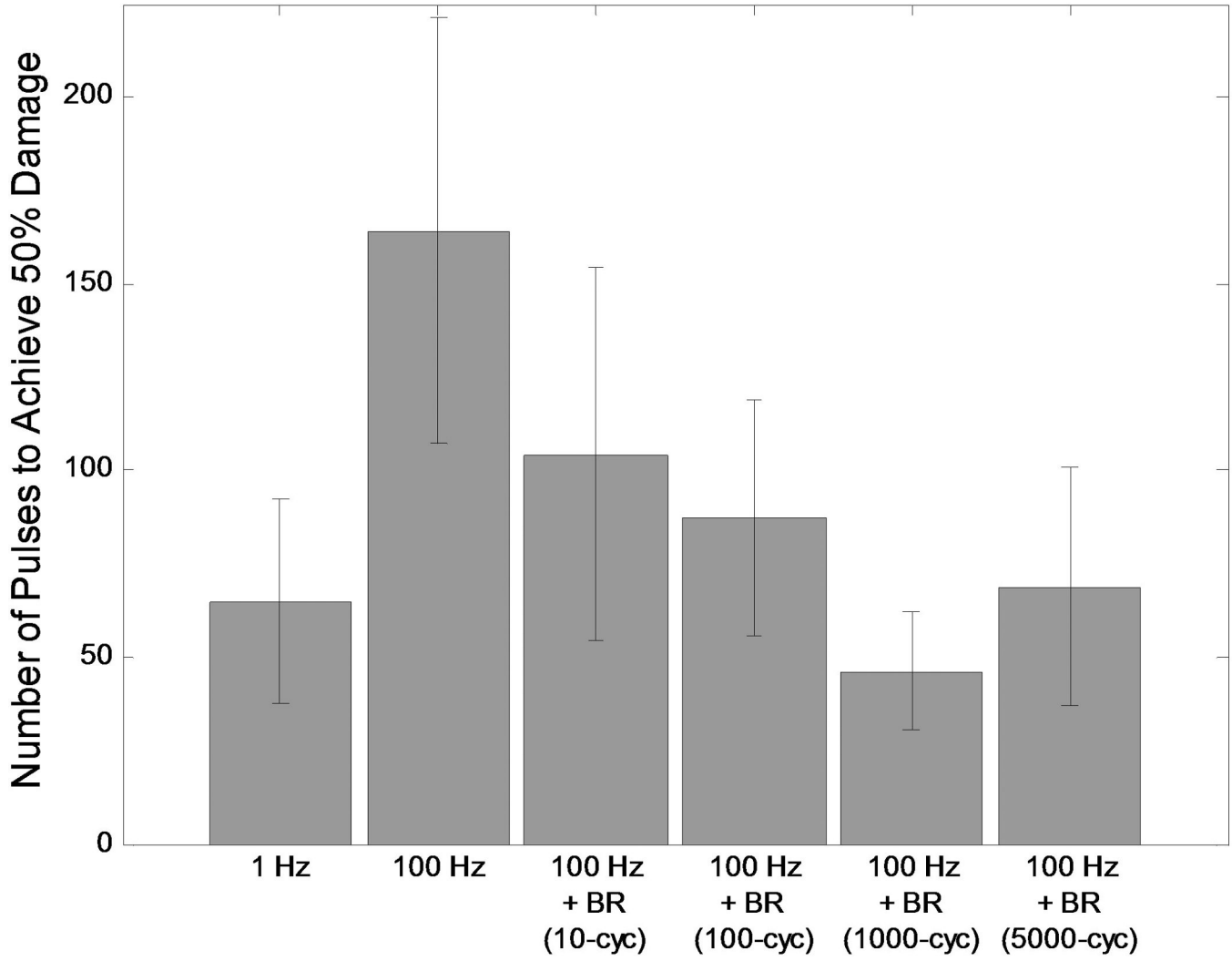

Fig. 7.

Number of histotripsy pulses required to achieve 50% fractionation within the reference zone, provided as a metric for the per-pulse efficiency of histotripsy lesion development. The low PRF of 1 Hz generated a high efficiency, requiring an average of only 65 pulses to reach the 50% damage level. Treatment at the high PRF of 100 Hz was much less efficient, with an average of 164 pulses needed for 50% damage. The incorporation of bubble removal sequences resulted in a reduction in the number of pulses required to reach the 50% damage level for all cases tested. Optimal efficiency was achieved with the incorporation of a 1000 cycle bubble removal sequence, which required an average of only 46 pulses to reach the 50% threshold.

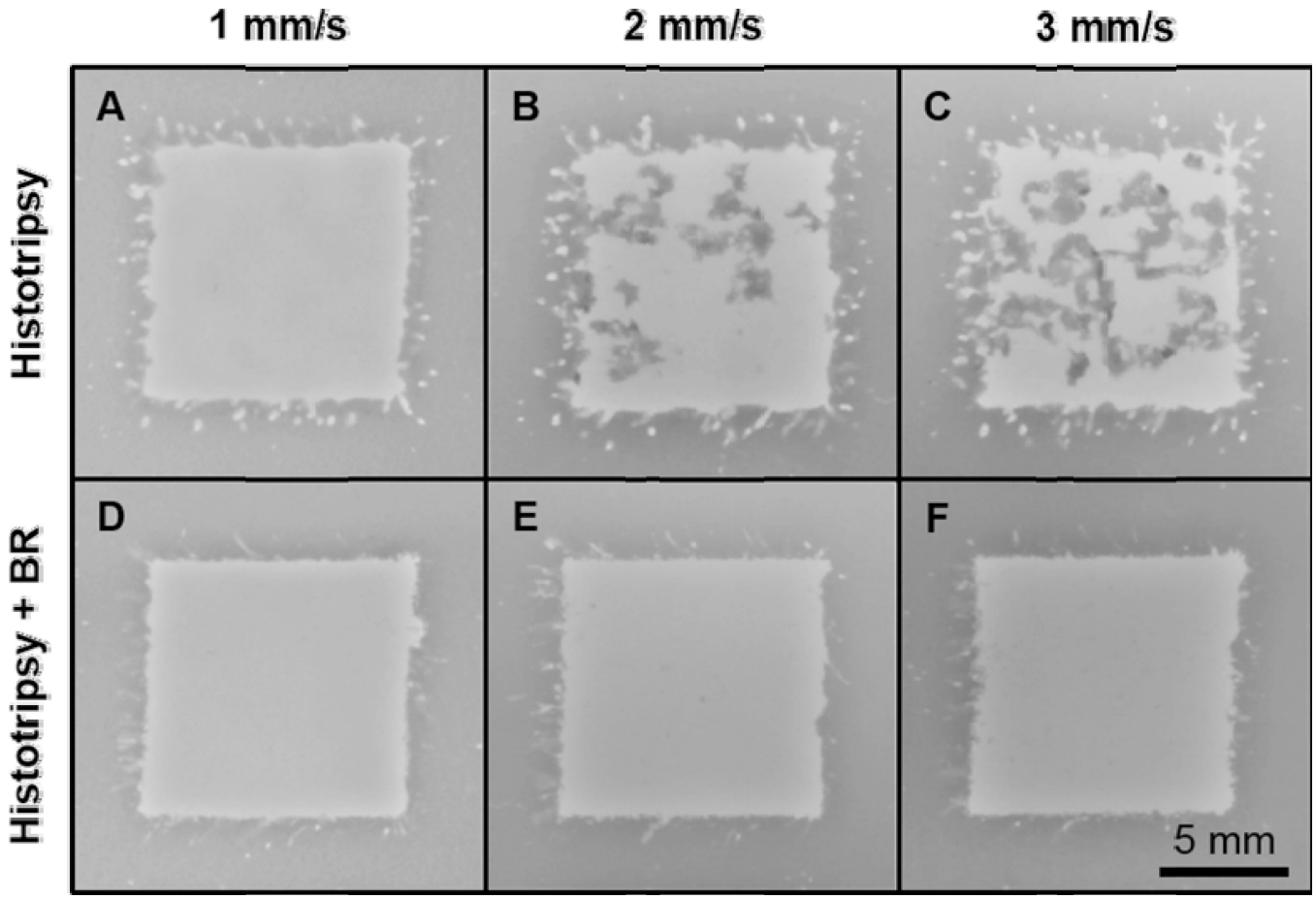

Fig. 8.

Representative volume treatments in the RBC tissue-mimicking phantom. (A–C) Without the incorporation of bubble removal sequences, as the linear scan speed was increased—i.e. as the histotripsy dose was lowered—the extent of intact tissue phantom structure remaining in the target zone increased. Speeds of 1, 2, and 3 mm/s resulted in average residual structure areas of 5.2, 24.1, and 40.5 mm^2, respectively. (D–F) With the incorporation of 1000 cycle bubble removal sequences, all histotripsy doses resulted in near-complete homogenization of the target zone. In this case speeds of 1, 2, and 3 mm/s produced average residual structure areas of 0.9, 4.0, and 3.8 mm^2, with the majority of this intact structure located on the perimeter of the target zone.